Proceedings of the 34th European Modeling & Simulation Symposium (EMSS), 031
18th International Multidisciplinary Modeling & Simulation Multiconference

2724-0029 © 2022 The Authors.
doi: 10.46354/i3m.2022.emss.031

Parametric model of a dielectric rod antenna array for terahertz applications

Anatoliy Prikhodko[1,2,*], Terentiy Yaropolov[1], Alexander Shurakov[1,2] and Gregory Gol'tsman[1,2]

[1]Moscow Pedagogical State University, 1/1 Malaya Pirogovskaya Str., Moscow, 119991, Russia
[2]National Research University Higher School of Economics, 20 Myasnitskaya ulitsa, Moscow, 101000, Russia

[*]Corresponding author. Email address: anatprikh1995@yandex.ru

Abstract

Mastering of the terahertz frequency band is attractive for numerous practical applications. Fabrication tolerances of widely used computer numerical control machining result in vital increase of input optics losses of active waveguide components at frequencies beyond 1 THz. This issue can be resolved if conventional hollow metallic waveguide technology is replaced by that making use of wave propagation in low-loss dielectric media. In this paper we report on the development of parametric model of a terahertz dielectric rod antenna array. Both analytic and numeric analysis for variety of the antenna array geometries are provided. The developed parametric model can be used to rigidly construct the dielectric rod antenna array with desired beam parameters at any frequency in the terahertz band if the antenna form factor is fixed and Si platform is used. We believe that our findings are of practical importance to terahertz photonics engineers.

Keywords: Dielectric rod antenna; antenna array; parametric model; terahertz band

1. Introduction

Optical transmission techniques rapidly migrate from visible light to radio frequencies (RF). This becomes a rigid trend in the last decade. Mastering of the terahertz (THz) band, i.e. frequencies from 0.1 to 10 THz, is attractive for the needs of communication and security systems, medical diagnostics, radio astronomy and climate studies. Fabrication tolerances of computer numerical control (CNC) machining result in vital increase of input optics losses of active waveguide components at frequencies beyond 1 THz. This issue can be resolved if conventional hollow metallic waveguide technology is replaced by that making use of wave propagation in low-loss dielectric media. Nowadays, design of such structures mostly relies on the use of electromagnetic (EM) simulation software (Al-Daffaie et al., 2022; Mukherjee et al., 2021). The software usually makes use of either the method of moments (MoM), finite element method (FEM) or finite-difference time-domain (FDTD) method (Gibson, 2021; Jin, 2015; Schneider, 2010). In this paper we report on the development of parametric model of a THz dielectric rod antenna (DRA) array. Both analytic and numeric analysis for variety of the antenna array geometries are provided. We believe that our findings are of practical importance to THz photonics engineers.

2. Dielectric rod antenna array

Concept of DRA is known to radio engineers for a long time (James, 1972; Shiau, 1976), yet DRA arrays have recently become of interest to scientific community due to their compatibility with the circuits of THz photonics relying on Si platform (Withayachumnankul et al., 2018a,b). The

existing DRA technology for THz applications is compatible with both step-index and photonic crystal waveguides. It provides capability of implementing simple linear and complex planar antenna arrays with nearly symmetric beam (Tesmer et al., 2019), but lacks universal analytic apparatus to rigidly construct geometry of DRA array with desired parameters. In this section we provide basic math, EM and parametric models for (i) a single DRA element and (ii) planar DRA array.

2.1. Basic math

For an antenna array of given geometry, multibeam interference of the elements in the far field region is accounted for with the aid of so-called array factor. In case of $M \times N$-elements planar antenna array with uniform amplitude and spacing (Balanis, 1997), the normalized array factor in spherical coordinates, $AF_{M,N}(\theta, \phi)$, is defined by equation 1. Note that the equation is provided for nullified phase increment between elements of the antenna array.

$$AF_{M,N}(\theta, \phi) = \frac{\sin(N\,\psi_x/2)}{N\sin(\psi_x/2)} \cdot \frac{\sin(M\,\psi_y/2)}{M\sin(\psi_y/2)} \qquad (1)$$

with $\psi_x = k_0 d_x \sin(\theta)\cos(\phi)$ and $\psi_y = k_0 d_y \sin(\theta)\sin(\phi)$, where k_0 is the free-space wavenumber, d_x is the spacing between the array elements along the x-axis and d_y is the spacing between the array elements along the y-axis.

Once intrinsic field pattern of each array element, $E_{el}(\theta, \phi, r)$, is known, one can evaluate the antenna array field pattern, $E_{\sum}(\theta, \phi, r)$, as

$$E_{\sum}(\theta, \phi, r) = AF_{M,N}(\theta, \phi) \cdot E_{el}(\theta, \phi, r). \qquad (2)$$

For the far field calculation case, when magnitude of position vector r is significantly greater than Fraunhofer distance, one can fix value of r in the dependence defined by equation 2 due to the wavefront planarity. As an example, figure 1 provides beam profile of 3×3-elements planar array of rectangular patch antennas acquired with the aid of the array factor method. In the calculation, uniform excitation amplitude and nullified phase increment are imposed on the equally spaced array elements. The spacing $d_x = d_y = \lambda/2$, where λ is the wavelength of interest. The calculation relies on analytic expression of the rectangular patch antenna field pattern, $E_{rp}(\theta, \phi, r)$, provided by equation 3.

$$E_{rp}(\theta, \phi, r) = \frac{ik_0\,h\,W\,E_0 e^{-ik_0 r}}{2\pi r} \cdot \frac{\sin(X)}{X} \cdot \frac{\sin(Z)}{Z} \cdot \gamma_1\gamma_2 \qquad (3)$$

with $X = -\frac{1}{2}\,k_0 h\,cos(\theta)$, $Z = \frac{1}{2}\,k_0 W\,sin(\theta)\,sin(\phi)$, γ_1 and γ_2 denoting coefficients defined by equations 4 and 5, respectively.

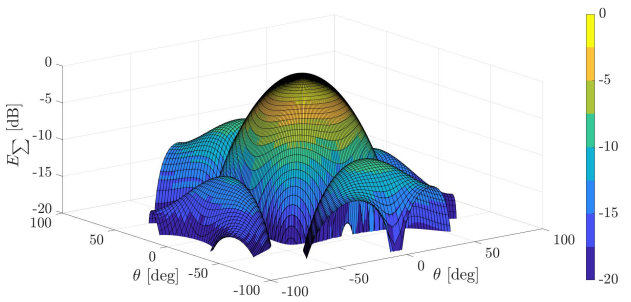

Figure 1. Normalized far-field beam profile of 3×3-elements planar array of rectangular patch antennas: $d_x = d_y = \lambda/2$, uniform excitation amplitude, nullified phase increment.

$$\gamma_1 = \sqrt{1 - [\sin(\theta)\,\sin(\phi)]^2} \qquad (4)$$

$$\gamma_2 = 2\cos[-\frac{1}{2}\,k_0 L_{eff}\,\sin(\theta)\,\cos(\phi)] \qquad (5)$$

Here h, W and L_{eff} are the height, width, and effective length of rectangular patch, respectively; E_0 is the magnitude of electric field. Note that we rearranged coordinates compared to those of classic expressions provided in (Balanis, 1997) and introduced ready-to-use equations 1–3 for properly aligned optical axes of the antenna elements with respect to the antenna array grid. Thus, one can easily predict properties of the antenna array beam in the far field region, once beam profile of the array element is known. Unfortunately, usability of the aforementioned approach suffers in case of DRA array. This is due to the complex EM behavior of DRA and, as a consequence, the lack of universal analytic model of the DRA beam profile in the THz band.

2.2. EM and parametric models

2.2.1. *Single antenna*

RF DRA is traditionally presented by a short section of dielectric step-index rectangular waveguide followed by a narrow-angle taper. It is quite natural to expect that there is a pronounced dependence of the DRA gain on the taper angle, α. This is not only important for defining optimal basic geometry of the antenna, but is vital in terms of fabrication tolerances too. The latter is even more severe in case of implementing a THz component. Thus, we conduct a series of 3D EM simulations for variety of the DRA geometries. Dielectric is presented by silicon, which has a relative permittivity of 11.9 and a loss tangent of 0 in our simulations. HFSS is used as a simulation software.

Figures 2 and 3 summarize outcome of the simulation of the DRA beam profile, *rEtotal*(θ), in E- and H-planes, when $\alpha \in \{2°, 4°, 6°, 8°, 10°\}$. In all the simulations, sig-

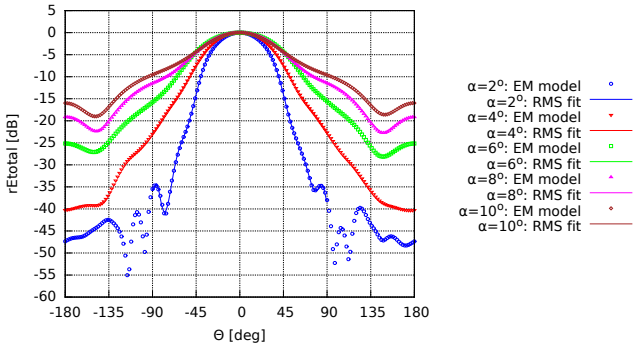

Figure 2. Normalized far-field beam profile of DRA in E-plane ($\phi = 0°$).

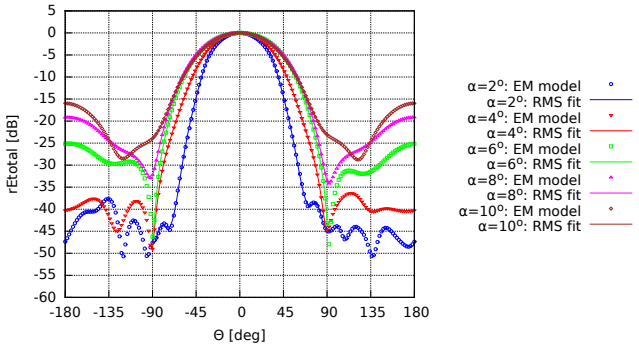

Figure 3. Normalized far-field beam profile of DRA in H-plane ($\phi = 90°$).

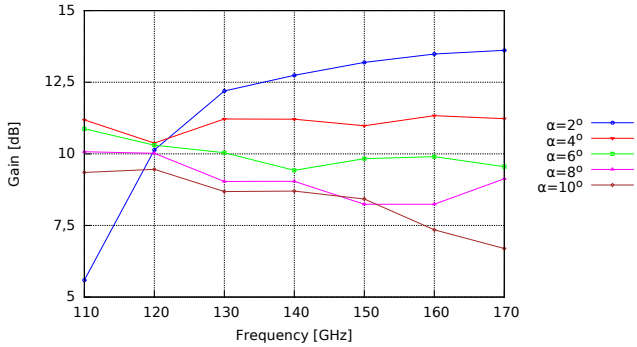

Figure 4. Gain of DRA as a function of frequency.

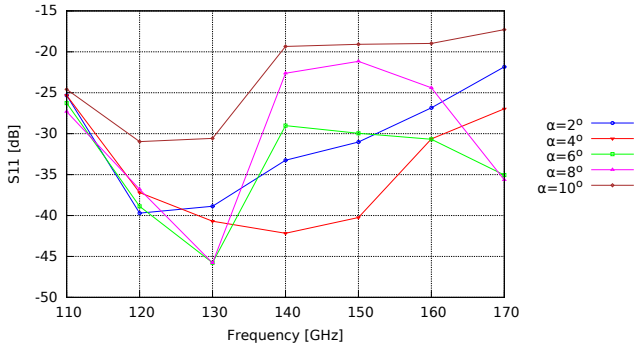

Figure 5. Frequency profile of DRA's *S*11.

nal frequency equals 140 GHz, cross-section of the antenna waveguide section is $a = 0.55$ mm $\times$ $b = 0.5$ mm (Width $\times$ Height) and it has a nearly zero length. One can clearly see that gradual decrease of the taper angle α results in narrowing of the beamwidth along with increase in the beam symmetry. Each simulated beam profile is approximated by a polynomial defined by equation 6 with the aid of the root mean square (RMS) method. Note that the fitting parameter c_j for the approximated beam profile, $rEtotal_{fit}(\theta)$, is measured in dB/deg^j.

$$rEtotal_{fit}(\theta) = \sum_{j=0}^{18} c_j \, \theta^j \qquad (6)$$

Results of the approximation for E- and H-planes are summarized in table 1. Corresponding beam profiles are also plotted in figures 2 and 3.

Figure 4 provides a series of frequency profiles of the DRA gain. A truly wide-band behaviour of the antenna is observed for $\alpha = 4°$ with almost constant value of its gain, which equals 11.2 dB at frequencies 110–170 GHz, i.e. over the entire WR6.5 band. The highest gain is equal to 13.7 dB and is achieved at 170 GHz for $\alpha = 2°$. For this geometry of DRA, input frequency range spans from 130 to 170 GHz. Yet, trend in the corresponding curve of figure 4 suggests usability of the antenna of such a geometry at even higher frequencies.

In all the aforementioned simulations, DRA is excited via wave port with a height of 0.83 mm and a width of 1.65 mm corresponding to the dimensions of a regular WR6.5 waveguide. To evaluate efficiency of the excitation, we calculate matrix of scattering parameters (S-parameters). Referring to figure 5, all the DRA geometries demonstrate decent matching with the excitation port and values of *S*11 stay well below -15 dB over the entire WR6.5 band.

2.2.2. *Planar antenna array*

Since DRA emits radiation from the entire outer surface of its narrow-angle taper, we decide to validate applicability of the math discussed earlier in section 2.1 for DRA array with sub-wavelength spacing between its elements.

Figure 7 provides beam profiles of 3×3-elements DRA array in E- and H-planes in case of half-wave spacing between the elements. The beam profiles are calculated with the aid of 3D EM modeling. To excite the array elements, we use wave port with a height $p_y = 3.5$ mm and a width $p_x = 3.55$ mm (see figure 6). Number of modes is set to 9, and each mode is associated with a corresponding array element via integration line. Thus, each integration line is drawn in the symmetry plane of the DRA taper within cross-section of the DRA input waveguide and collinear with the taper tip. Such a setup enables modeling with (i) uniform excitation amplitude and (ii) nullified phase

Table 1. Results of the DRAs beam profiles approximation for E- and H-planes.

	E-plane:					H-plane:				
c_j	α = 2°	α = 4°	α = 6°	α = 8°	α = 10°	α = 2°	α = 4°	α = 6°	α = 8°	α = 10°
c_0	1.307E-02	-4.802E-03	5.716E-05	1.077E-04	1.313E-04	2.263E-01	-9.946E-03	-2.217E-02	-1.322E-03	-4.245E-04
c_1	-1.057E-02	7.048E-04	1.474E-04	9.886E-05	-4.352E-04	4.525E-04	-1.128E-03	-6.132E-03	1.719E-04	7.130E-04
c_2	-4.257E-03	-2.558E-03	-1.830E-03	-2.039E-03	-2.399E-03	-9.637E-03	-2.587E-03	-1.554E-03	-1.971E-03	-2.309E-03
c_3	7.426E-05	2.120E-06	4.076E-07	1.545E-07	-5.401E-08	-5.890E-06	1.630E-06	4.190E-05	-1.547E-06	-5.009E-07
c_4	-1.503E-06	-1.087E-06	-9.274E-08	-2.125E-07	3.055E-08	2.041E-05	-1.496E-06	-2.122E-06	-3.316E-07	-2.283E-07
c_5	-1.533E-07	-4.286E-09	-7.062E-10	1.805E-10	1.361E-10	6.455E-10	-3.080E-09	-8.376E-08	3.043E-09	2.689E-10
c_6	3.999E-09	6.049E-10	-9.116E-11	4.665E-11	3.233E-11	-2.992E-08	1.122E-09	2.831E-09	1.777E-10	5.586E-11
c_7	1.399E-10	3.831E-12	5.502E-13	-2.302E-13	-4.226E-14	1.310E-11	1.821E-12	7.469E-11	-2.807E-12	-2.726E-13
c_8	-5.832E-12	-3.312E-13	6.007E-14	1.389E-14	2.478E-14	1.978E-11	-7.622E-13	-2.094E-12	-1.520E-13	-4.003E-14
c_9	-6.634E-14	-1.871E-15	-2.200E-16	7.706E-17	-6.338E-18	-1.244E-14	-3.555E-16	-3.494E-14	1.340E-15	1.441E-16
c_{10}	3.346E-15	1.236E-16	-2.600E-17	-5.345E-18	-1.344E-17	-7.228E-15	3.129E-16	8.471E-16	6.836E-17	1.701E-17
c_{11}	1.736E-17	4.919E-19	4.848E-20	-1.069E-20	4.023E-21	4.731E-18	-6.204E-20	9.189E-18	-3.578E-19	-4.038E-20
c_{12}	-9.480E-19	-2.525E-20	7.231E-21	8.042E-22	2.818E-21	1.538E-18	-7.560E-20	-1.983E-19	-1.754E-20	-4.041E-21
c_{13}	-2.513E-21	-6.945E-23	-5.800E-24	5.396E-25	-5.854E-25	-8.692E-22	3.478E-23	-1.365E-21	5.405E-23	6.530E-24
c_{14}	1.424E-22	2.764E-24	-1.095E-24	-6.799E-26	-3.107E-25	-1.887E-22	1.069E-23	2.678E-23	2.586E-24	5.366E-25
c_{15}	1.879E-25	4.981E-27	3.483E-28	8.876E-30	3.493E-29	7.694E-26	-4.851E-27	1.067E-25	-4.320E-27	-5.551E-28
c_{16}	-1.089E-26	-1.520E-28	8.295E-29	3.134E-30	1.789E-29	1.235E-26	-8.193E-28	-1.932E-27	-2.046E-28	-3.604E-29
c_{17}	-5.662E-30	-1.430E-31	-8.125E-33	-1.203E-33	-7.276E-34	-2.636E-30	2.274E-31	-3.410E-30	1.414E-31	1.882E-32
c_{18}	3.337E-31	3.254E-33	-2.479E-33	-5.966E-35	-4.253E-34	-3.338E-31	2.618E-32	5.755E-32	6.732E-33	9.417E-34

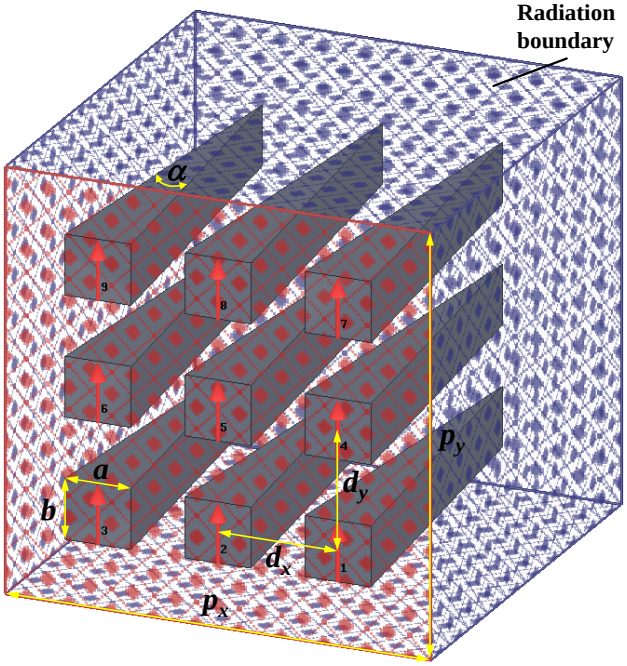

Figure 6. 3D HFSS model of 3 × 3-elements DRA array.

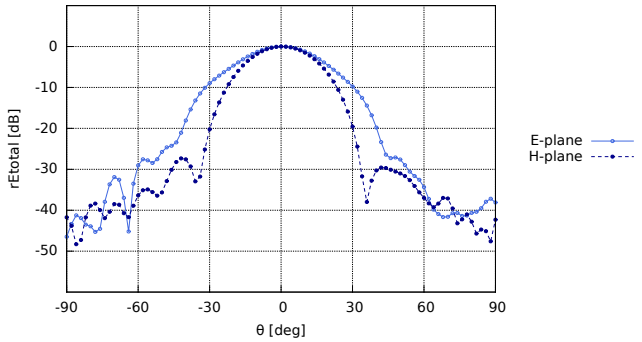

Figure 7. Normalized far-field beam profile of 3 × 3-elements DRA array: α = 2°, $d_x = d_y = \lambda/2$, uniform excitation amplitude, nullified phase increment, calculated via 3D EM modeling.

increment between elements of the array. The calculation is carried out for signal frequency of 140 GHz and the taper angle α = 2°. As one can naturally expect, the simulated beam profiles are noticeably narrower compared to those of a single DRA (see figures 2 and 3 for details).

In turn, figure 8 illustrates beam profile of the aforementioned DRA array calculated with the aid of equations 2 and 6. As one can clearly see, the E-plane beam profile is in decent agreement with that provided in figure 7. And the H-plane beam profiles demonstrate similarity acceptable from a practical point of view. Thus, we conclude that parametric model of DRA provided in section 2.2 combined with the array factor method results in ready-to-use parametric model of DRA array. The latter can be used to rigidly construct geometry of DRA array with desired parameters. This is possible not only within the frequency range of 110–170 GHz, but at any frequency in the THz band if the DRA form factor is fixed and Si platform is used.

3. Conclusions

Our study is devoted to the development of parametric model of a THz DRA array. Since DRA emits radiation from the entire outer surface of its narrow-angle taper, we decide to validate applicability of the array factor math for DRA array with sub-wavelength spacing between its elements. In the manuscript we provide both analytic and numeric analysis for variety of the DRA geometries. These include calculations of (i) the antenna beam profiles and

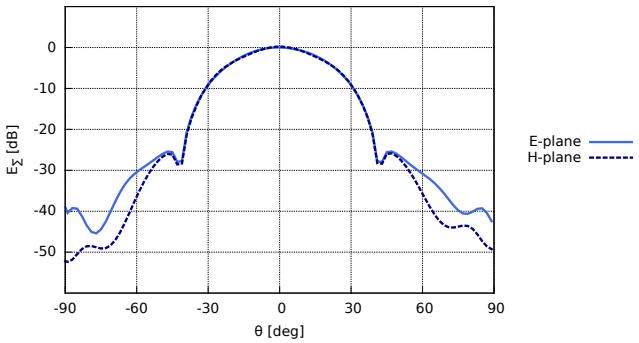

Figure 8. Normalized far-field beam profile of 3×3-elements DRA array: $\alpha = 2^\circ$, $d_x = d_y = \lambda/2$, uniform excitation amplitude, nullified phase increment, calculated via equations 2 and 6.

matrices of scattering parameters at signal frequency of 140 GHz, (ii) frequency profiles of the antenna gain over the entire WR6.5 band. The obtained results together with the array factor method are used to build a parametric model of DRA array. The developed model can be used to rigidly construct geometry of the array with desired beam parameters at any frequency in the THz band if the antenna form factor is fixed and Si platform is used. We believe that our findings are of practical importance to THz photonics engineers dealing with energy transfer from integrated circuits into a free space (and vice versa). Use of the developed parametric model enables independent design of input/output coupling optics and complex on-chip circuitry, aids to decrease calculation time noticeably.

4. Funding

The study was supported by the Russian Science Foundation grant No. 22-79-10279, https://rscf.ru/project/22-79-10279/.

References

Al-Daffaie, S., Jumaah, A. J., Rubio, V. L., and Kusserow, T. (2022). Design and implementation of a terahertz lens-antenna for a photonic integrated circuits based thz systems. *Scientific reports*, 12(1):1–7.

Balanis, C. A. (1997). *Antenna theory: analysis and design*. John wiley & sons.

Gibson, W. C. (2021). *The method of moments in electromagnetics*. Chapman and Hall/CRC.

James, J. R. (1972). Engineering approach to the design of tapered dielectric-rod and horn antennas. *Radio and Electronic Engineer*, 42(6):251–259.

Jin, J.-M. (2015). *The finite element method in electromagnetics*. John wiley & sons.

Mukherjee, A. K., Xiang, M., and Preu, S. (2021). Broadband terahertz photonic integrated circuit with integrated active photonic devices. *Photonics*, 8(11):492.

Schneider, J. B. (2010). *Understanding the finite-difference time-domain method*. School of electrical engineering and computer science Washington State University.

Shiau, Y. (1976). Dielectric rod antennas for millimeter-wave integrated circuits (short papers). *IEEE Transactions on Microwave Theory and Techniques*, 24(11):869–872.

Tesmer, H., Reese, R., Polat, E., Nickel, M., Jakoby, R., and Maune, H. (2019). Fully dielectric rod antenna arrays with integrated power divider. *Frequenz*, 73(11-12):367–377.

Withayachumnankul, W., Fujita, M., and Nagatsuma, T. (2018a). Integrated silicon photonic crystals toward terahertz communications. *Advanced Optical Materials*, 6(16):1800401.

Withayachumnankul, W., Yamada, R., Fujita, M., and Nagatsuma, T. (2018b). All-dielectric rod antenna array for terahertz communications. *APL Photonics*, 3(5):051707.